JOURNAL OF MATERIALS SCIENCE **39** (2004) 4575–4586

Effects of designed tubular porosity on compressive strengths of honeycomb ceramics

ASHWIN HATTIANGADI, AMIT BANDYOPADHYAY
School of Mechanical and Materials Engineering, Washington State University, Pullman, WA, 99164, USA
E-mail: amitband@wsu.edu

Three-dimensional honeycomb porous ceramics were fabricated using the fused deposition process. The structures were designed to have a controlled interconnected porosity. Elastic interactions between pores of honeycomb ceramic materials were then evaluated for different pore parameters using the finite element modeling (FEM) approach. The FEM results were compared experimentally with the compressive failure strengths of the honeycomb ceramics. The effect of relevant pore parameters on the compressive strength was studied. An analytical fracture mechanics based approach is presented for comparison with the FEM to reflect on the relative importance of pore parameters for different volume fractions of porosity. A detailed insight is also provided into the interrelation between various porosity parameters, mechanical behavior and design of these structures.

Φ_{th}	Theoretical volume fraction porosity
Φ_{exp}	Experimentally measured volume fraction porosity
W	Road width in polymer mold (or) Pore width in porous ceramic structure
H	Slice thickness in polymer mold (or) Pore height in porous ceramic structure
I	Raster gap in polymer mold (or) Horizontal pore-pore interaction distance between pores
S	Pore shape
Z	Pore size
σ_{comp}	Maximum compressive failure stress
$\sigma_{tension}$	Maximum tensile failure stress
R	Stress ratio $= \sigma_{comp}/\sigma_{tension}$
ESIP	Effective stress interaction parameter
SCF	Stress concentration factor $= \sigma_\theta/\sigma_{applied}$
σ_θ	Stress on pore boundary
R_{pore}	Stress ratio along pore boundary

1. Introduction

Porous ceramic materials have a wide range of applications that includes fuel cell separators, biological media, bone grafts, catalytic supports, filters and gas sensors [1–3]. Porosity in ceramic structures divides them into two types-high or low density. High-density porous ceramics exhibit volume porosity less than 30%, depending on the stacking sequence of ceramic particles. This porosity is formed by partial sintering at controlled temperatures [3–8]. Low-density porous ceramics with volume porosity greater than 70% are also called foams or cellular solids. They are formed by pore forming agents [2, 9–11]. The porosity in these high and low-density porous materials is commonly random in nature.

Theoretical and experimental characterization of porous materials is not new; several theories have been postulated to characterize the mechanical strength and strength degradation due to random porosity of polycrystalline ceramics [12–18]. Successful models are available for low density cellular solids [2, 19–22]. For materials with high density (above 0.3 of theoretical) several theories have been postulated to explain strength degradation. These theories can be classified into three broad categories: (1) reduction in cross-section area, (2) stress concentration and (3) effective flaw size. There have been several studies of the effect of porosity on mechanical strength, but none have been definitive [3]. Arguments presented in support of this view are: (a) the variable nature of stress concentrations for isolated pores, (b) the interactive nature of stress concentrations because of porosity in which pores were no longer isolated and (c) the interaction of pores and cracks. There are also equations cited in the literature that have been used to fit experimental results from porous solids. They are generally based on empirical constants that are related to the volume fraction porosity, and are applicable only for certain materials processed under specific conditions. A need exists for modeling to be carried out with a broader perspective on porous structures.

In this paper, two popular modeling approaches are evaluated and their ideas are combined in a more general finite element scheme to model non-random porous materials. Modeling techniques using the minimum solid area (MSA) across "random" porous ceramics are used to characterize decrease in modulus with increase in porosity [34, 35]. Likewise, modeling using

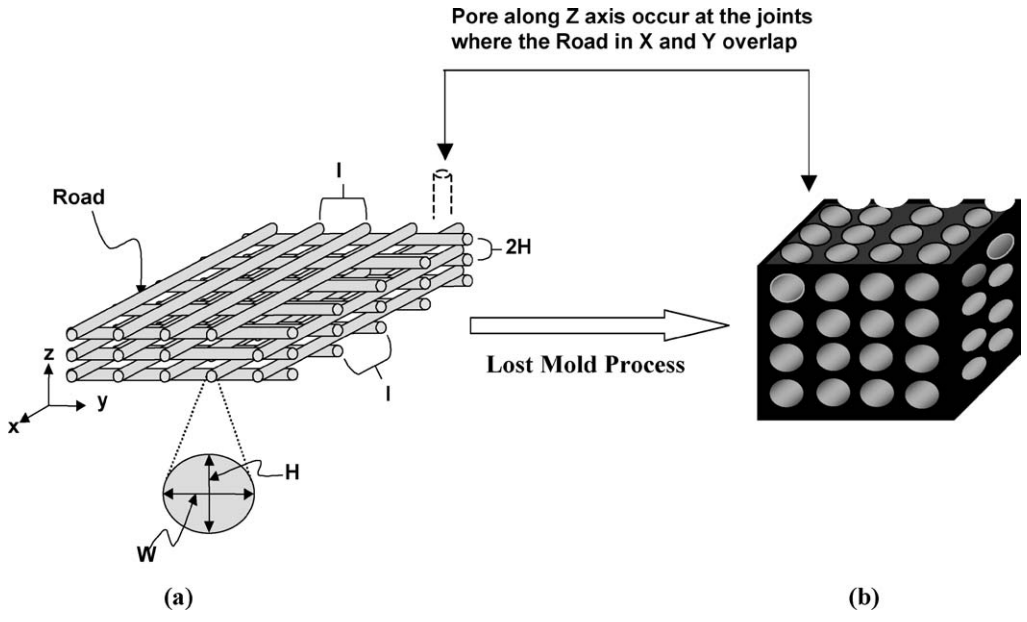

Figure 1 Indirect FDM processing technique. (a) Internal architecture of polymer mold. (b) 3D honeycomb porous structure. Figures plotted not to scale.

fracture mechanics has been used to study crack growth using stress intensity factors between specified numbers of pores in ductile as well as brittle solids. In this paper an analytical expression for stress intensity factor is derived for multiple pores to identify the critical porosity parameter for a wide range of porosity. The analytical model is extended by using the **f**inite **e**lement **m**ethod (FEM) approach to evaluate stresses around a pore and interactions between stresses for multiple pores for non-random porous structures. Using the FEM, a two-pore material system was found to be sufficient to represent multiple pores especially due to the non-randomness of the pores [23]. Calculated values were verified with experimental data for controlled honeycomb porous structures with designed tubular porosity. These controlled porosity structures were processed using the indirect fused deposition process, a commercially available **s**olid **f**reeform **f**abrication (SFF) technique [24, 25].

The FEM technique is extended in this paper to study the interrelation between various porosity parameters and compressive strengths of 3D honeycomb ceramic materials. Three dimensional honeycomb materials have interconnected cylindrical pores along a defined X, Y and Z-axis direction. The processing method allowed for pores of specific shape, size and connectivity to be designed, thereby allowing control over the volume fraction porosity as well. Some discussion is also presented on the dependence of these properties on processing methods and microstructural parameters. The FEM technique shows good agreement with the experiment results. The result from numerical FEM approach shows that for wide ranges of porosity, different pore parameters contribute to failure, thereby agreeing well with outcome from the analytical fracture mechanics model.

2. Processing

Fused **d**eposition (FD) process is one of the commercial SFF processes developed by Stratasys Inc. (Eden Prairie, MN). In this process a thermoplastic filament is extruded onto a horizontal platform to form a single layer of material. Once a single layer is deposited, the platform moves down and deposition of the next layer on the previous layer starts. The process continues till a complete structure is built, based on its CAD information.

The SFF techniques can be used to fabricate functional metal/ceramic parts or prototypes in two ways: (a) the direct and (b) the indirect route. In the direct route, green metal/ceramic components are fabricated directly from their CAD file using an SFF process [26]. In the indirect route, a polymer mold of the desired structure is fabricated via an SFF process. The positive is then cast using a metal/ceramic powder-based slurry/gel, via a lost mold technique. In this study, an indirect process was used where polymeric molds were fabricated using FDM 1650 machine. Mullite powder[1] of -325 mesh size was used, with additives, to form the water-based slurry. The slurry development has been reported elsewhere [27, 28]. After the infiltration of the porous molds, the samples were dried, binder was removed, and they were pressureless-sintered to obtain the 3-D honeycomb structures. A different pore architecture was obtained by custom designing the molds. The schematic of internal architecture of polymer mold obtained through FD which results in a non-random porous structure is shown in Fig.1.

Fig. 1a shows the FD extruded single deposit called a "road", which has a width (W) and height (H). The horizontal distance between the roads is called as road gap (I). Fig. 1b shows the 3D honeycomb ceramic formed, via the lost mold technique, which exhibits cylindrical pores with width and height determined by the road width (W) and the road height (H). The horizontal pore-pore interaction is imparted by the road gap (I). Using this processing route, non-random porous

[1]MULCOA, C. E. Minerals, PA, USA.

structures were formed in the range of 21–47% porosity with controlled pore size, shape and connectivity.

3. Modeling of porous structures

3.1. Minimum solid area

Minimum solid area method (*MSA*) is popular to characterize failure of random porous structures [34, 35]. For the tubular designed 3-D porous ceramics used in this study the pore interaction distance (I) represents the *MSA*. However, it should be emphasized that the change in pore width (W) can be an important parameter, since it causes change in shape (S) and a non-uniform change in size (Z). The *MSA*/pore interaction distance would be limited in characterizing a porous ceramic when the minimum solid cross-section across the porous ceramic is constant while the change in volume fraction porosity is achieved by modifying the pore shape and not the pore-pore distance, which affects the failure strength of porous bodies. Therefore the *MSA*/pore interaction distance approach by itself would not be able to fully capture the critical failure parameter for different volume fractions of porosity, if the *MSA* does not affect the change in volume fraction porosity. The effect of W needs to be accounted while modeling a porous material, although it can be difficult to predict the exact contribution of W and I on strength degradation especially for a random porous ceramic. A statistical study of variance of the experimental and numerically obtained stress values for 3D honeycomb porous ceramics shows that the significance of W is in fact slightly more than I on the strength degradation for certain pore geometries [36]. Therefore it is essential to look at other modeling techniques such as the fracture mechanics based approach or the numerically based FEM approach to characterize *non-random* porous ceramics. The *MSA* model by itself would be insufficient to explain the failure of porous ceramics for different pore volumes and failure strengths caused primarily by pore widths and shapes.

3.2. Fracture mechanics based approach

Fracture mechanics based approaches use analytical solutions to evaluate stress interactions and thus effective stress intensity factors for a pore or multiple pores in an infinite medium. From the Griffith theory of fracture mechanics for a *sharp crack* the stress intensity factor K is obtained as,

$$K = \sigma\sqrt{\pi a} \tag{1}$$

where σ is the gross applied stress and a is half the length of the crack. The material is capable of withstanding only a certain K value before fracturing. Therefore at fracture,

$$K = K_{cr} \Rightarrow \text{Fracture}$$

The constant K is the measure of the strength of the stress field near a crack and is therefore referred as the stress intensity factor (*SIF*). Higher the value of K, higher is the probability of fracture.

Consider cracks of length ($2a$) are spaced at distance $2b$ units apart; i.e. centerlines are $2b$ units apart shown in Fig. 2a. The surfaces of the cracks must be stress free. The following boundary conditions can be applied,

(1) $\sigma_y = 0$ @ $y = 0$ for $|x| < \pm a$
(2) $\sigma_{xy} = 0$ @ $y = 0$ for all x

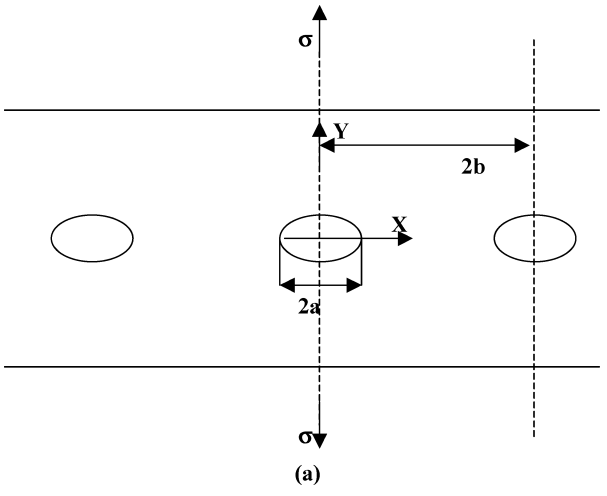

(a)

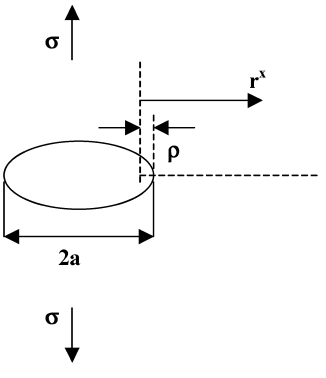

(b)

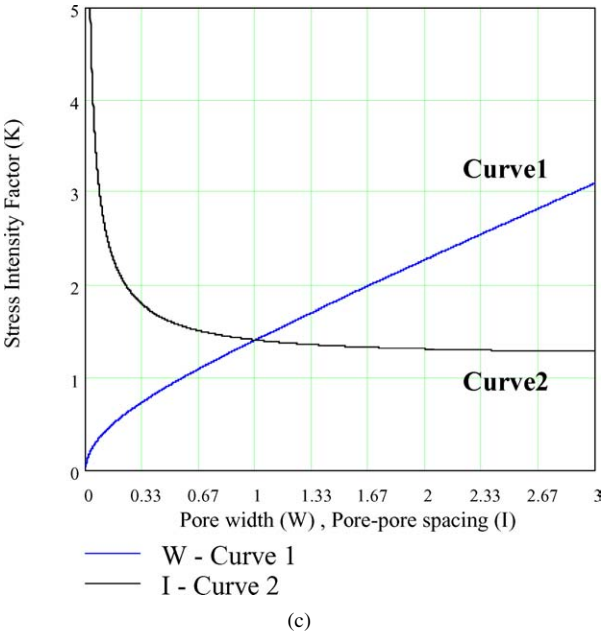

(c)

Figure 2 (a) Horizontal periodic cracks in a infinite plate subjected to tensile loading along the Y-axis (b) Crack of length 2a and a radius of curvature ρ at the tips. (c) Stress intensity factor as a function of the pore width and pore-pore spacing.

(3) $\tau_{xy} = 0$ for $x = \pm(2n-1)b$, $n = 1, 2, 3$, etc.
(4) For infinite plate, $\sigma_y = \sigma$ for $z \to \infty$

For finite plate, $\sigma_y = \sigma$ for $z \to$ finite boundary, such that the solution is holomorphic in the finite domain.

An appropriate stress function for this problem can be expressed as,

$$z = \frac{\sigma \sin\left(\frac{\pi z}{2b}\right)}{\sqrt{\sin^2\left(\frac{\pi z}{2b}\right) - \sin^2\left(\frac{\pi a}{2b}\right)}} \tag{2}$$

The expression for the stress intensity parameter can be derived using conformal mapping and fracture mechanics techniques as,

$$K = \sigma\sqrt{\pi a}\sqrt{\frac{2b}{\pi a}\tan\left(\frac{\pi a}{2b}\right)} \tag{3}$$

This analysis also allows for a stress intensity factor for a specimen of finite size. When $2b > 2a$, the change in K is not observed. Based on this philosophy, an analogy with the modeling approach adopted in this study can be derived.

The analysis presented above considers pore as a crack. Introducing a radius of curvature (ρ) to the crack as shown in the Fig. 2b, an analytical solution for periodic elliptical pores in a plate can be developed. For a sharp crack, $\sigma_y = \sigma_{max.}$ at the crack tip. When $r^x = \rho$, the maximum stress would be,

$$\sigma_{max} = \sigma_y = 2\sigma\sqrt{\frac{a}{\rho}} \tag{4}$$

This expression can be written as

$$\sigma_y = \frac{c}{\sqrt{\rho}}\frac{K}{\sqrt{2\pi r^x}} \tag{5}$$

Here the radius of curvature (ρ) can be expressed as, $\rho = \frac{b^2}{a}$. When $r^x = \rho$ we get,

$$2\sigma\sqrt{\frac{a}{\rho}} = \frac{c}{\sqrt{\rho}}\frac{\sigma\sqrt{\pi a}}{\sqrt{2\pi\rho}} \tag{6}$$

Hence the constant, c, can be found as, $c = 2\sqrt{2\rho}$. Therefore from the earlier expression of the maximum stress of sharp crack, an expression for an elliptical crack with a radius of curvature is found as,

$$\sigma_y = \frac{2K}{\sqrt{\pi r^x}} \tag{7}$$

The stress intensity factor (K) is the same as that of the sharp crack presented in Equation 3. This equation can be expressed in terms of pore parameters, pore width (W) and pore-pore interaction distance (I). The pore width (W) is equal to the length of the elliptical crack ($2a$) and the center-center distance of pores ($2b$) is equal to the sum of pore-pore interaction distance (I) and W. Therefore K is obtained as,

$$K = \sigma\sqrt{\pi\frac{W}{2}}\sqrt{\frac{2(I+W)}{\pi W}\tan\left(\frac{\pi W}{2(I+W)}\right)} \tag{8}$$

The variation of K as a function of pore parameters, W and I is shown in Fig. 2c. For *curve 1*, the distance between periodic elliptical cracks I was maintained constant at 1 *unit* and the width (W) was increased from 0 to 3 *units.* The stress (σ) was chosen as 1 *unit* to evaluate the stress intensity factor (K). When W is small for a large I, the plate with periodic elliptical cracks represents a high-density solid with microporosity of 0 to 50 volume percent. It can be observed from *curve 1* that the K value increases steadily (constant slope) as the pore width increases. This suggests that W is the critical parameter for failure of high-density solids.

As W is increased maintaining a constant I value, the plate with pores represent a cellular solid. The *curve 2* shows the variation of K with change in I for a constant W value. In *curve 2*, W is maintained constant at 1 *unit* and I is varied from 0 to 3 *units*. It can be observed that as I decreases with respect to W, the stress intensity increases exponentially. This suggests that I is the critical parameter for failure of low-density solids. If both W and I are considered as critical parameters for failure, a variation in stress intensity K may not be observed for the change in W or I. This suggests that for certain porosity depending on its range, either W or I act as the critical parameter in failure as seen in this analysis. From the modeling approach proposed in this paper, similar results are seen as described in the following sections.

To understand the influence of the different pore parameter on failure, numerical approach using FEM is needed. Such a study is presented in more details in the following sections.

3.3. Numerical modeling using FEM

3.3.1. Two-dimensional model of failure plane

Compressive strength of porous materials is generally not controlled by single or isolated pores, since compressive failure is typically one of cumulative damage or cracking [3]. This is in contrast to tensile failure, in which catastrophic failure from the single weakest flaw is the case. Isolated pores or clusters are believed to have less effect in compression. The high stresses and progressive failure in compression may provide opportunity for pore shape and stress concentrations to come into play via progressive cracking as load increases [25]. This may increase the porosity-dependence of compressive strength.

The failure of porous cylinders under axial compression occurs by *vertical slabbing*, wherein microcracks grow or combine to form contiguous vertical failure planes [29]. The brittle porous structures discussed here have cylindrical pores interconnected in the X, Y and Z-directions as shown in Fig. 1. In the presence of micropores in ceramic, anisotropy of tubular porosity in the X, Y and Z directions would play a role. Failure

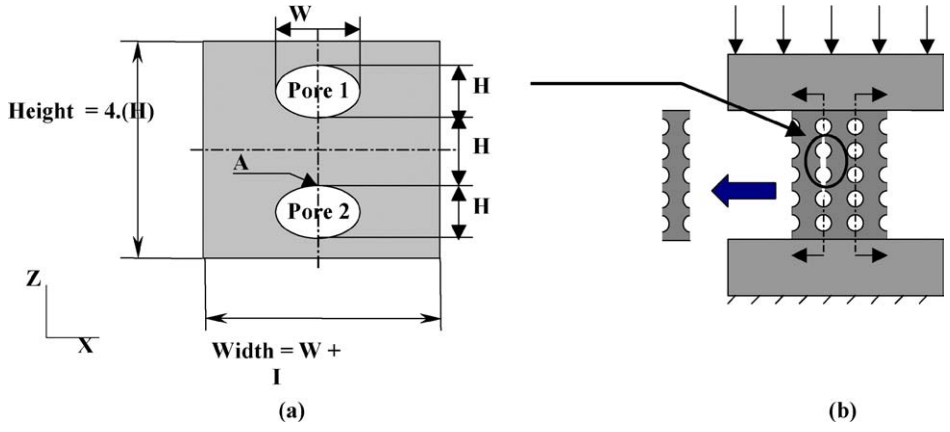

Figure 3 (a) Schematic of two pore model of the honeycomb porous ceramic structure. (b) Proposed failure plane for tubular porous structures.

would occur along a skewed plane which is a combination of planes that are horizontally perpendicular and vertical parallel to the direction of loading. Based on the assumption that micropores in ceramic are negligible it can be confidently assumed that under compression failure planes form vertically parallel to the loading direction and the samples fail by brittle crushing. In this study the cylindrical pores along the horizontal X and Y-direction are perpendicular, so a two-dimensional representation of vertical failure planes can be used to model the failure of the 3D structure.

The two dimensional representation of one such plane through which failure occurs is shown in Fig. 2, in which the volume fraction porosity (Φ) is represented in 2-D as areal fraction of porosity (A_{th}). An equation for the theoretical volume fraction porosity (Φ_{th}) of a non-random porous structure has been derived elsewhere [23]. It is expressed in terms of A_{th} in Equation 1,

$$\Phi_{th} = \frac{2(n+2)}{n}\left(\frac{\pi W}{8(W+I)}\right) \quad \text{or}$$

$$\Phi_{th} = \frac{2(n+2)}{n}(A_{th}) \tag{9}$$

where, n is an arbitrary real number and A_{th} is the areal fraction of Φ_{th}. For $n = 15$, the stereological constant of proportionality, $2 \cdot (n+2)/n$, is obtained as 2.26. This value is retained for all porosities used in this study. This constant can be calculated by assuming a large value for the arbitrary real number (n) or correlating Equation 9 with one porosity value obtained experimentally for a known pore geometry.

3.3.2. Evaluation of tensile stresses

The basic concept of the FEM approach has been explained elsewhere [23]. It is observed that on vertical failure planes, failure zones are formed at locations on the pore boundaries where the tensile stresses are maximum. Since tensile failure occurs for ceramics and other brittle solids at a much smaller load than compressive failure, porous brittle structures loaded in compression fail at regions where tensile stresses are maximum. A stress ratio (R) defined for brittle materials (compression over tension) gives an indication of how the material behaves when loaded in a particular way. For most brittle solids (R) is greater than 10. This suggests that porous brittle materials may fracture predominantly due to tensile stresses at pore boundaries.

Since interacting tensile stresses at pore boundaries are prominent in causing failure, they are used to model failure in brittle porous solids, subjected to compressive loading. The maximum tensile stress along the boundary of pore 2 in Fig. 3a is $\sigma_A(\Phi_{th}, B)$ at point A. Here, $\sigma_A(\Phi_{th}, B)$ is the enhanced tensile stress component due to the interaction of pore 2 with pore 1 and B represents boundary effects to account for interaction of pore 2 with neighboring pores. Boundary effects account for location of pores and are a physical representation of behavior in a multiple pore system. Moreover, experiments have shown that cracks interact with the surface of a finite sample in a way, which causes them to grow faster than they do in an infinite medium [30].

The maximum tensile stress on the pore boundary of pore 2 when pore 1 is not present can be evaluated as $\sigma_B(\Phi_1, B_1)$, where Φ_1 and B_1 are effective porosity and finite boundary respectively, when there is no pore-pore elastic interaction. The Φ_1 and B_1 are directly proportional to Φ_{th} and B respectively, for particular pore geometry, i.e.,

$$\Phi_1 \alpha \Phi \quad \text{and} \quad B_1 \alpha B$$

Therefore the effective stress interaction on pore 2 is evaluated as the ratio of $\sigma_A(\Phi_{th}, B)$ to $\sigma_B(\Phi_1, B_1)$. This unitless parameter can be called the **e**ffective **s**tress **i**nteraction **p**arameter or *ESIP*. By evaluating *ESIP* values for different pore geometries and volume fraction porosities, the multiple pore material system can be modeled. When multiplied by a constant M for a particular material system and processing conditions, the failure stress of porous ceramics is obtained. It is worth noting at this point that the analysis is an upper bound solution in which the effects of microporosity are not considered. The constant M is the value at which the brittle solid with no interaction between pores will fail under uniaxial tensile loading ($\sigma_{tension}$). The value of M is dependent on factors such as the material system, processing method, and grain size and distribution. It has a *fixed* value when these factors are kept constant.

4. Boundary conditions, loading and material properties

The two-dimensional FE analysis was carried out on the commercial software ANSYS ver. 5.4. Plates with pores were meshed by triangular 2-D elements; typically the number of elements varied from 150 to 200 to obtain a converged solution. The boundary conditions were set such that nodes along the bottom edge were fixed in the Z-direction but were allowed to move in the X-direction, except for the node at one of the bottom corners, which was fixed in the X-direction to prevent rigid body motion. A compressive load of unit intensity was applied to the mesh in the Z-direction. Young's modulus and Poisson's ratio were selected as 145 GPa (0.21×10^8 psi) and 0.24, respectively, from the CRC materials handbook for mullite. The plates with pores were analyzed using the p-method and convergence of the strain energy at specified nodes at point A of Fig. 2 was set at 0.5% [31]. The 2-D FEA were carried out in plane stress and plane strain; since stress values did not vary greatly, plane strain method was adopted and reported.

5. Experimental method

Cylindrical porous mullite samples 25 mm long and 15 mm in diameter, which had been fabricated using the processing method described, were subjected to uniaxial compressive loading. Green samples were polished on the top and bottom surfaces to make them parallel before firing. Sintered samples were tested under compressive loading without any further machining operation. Samples were placed in a way that one set of tubular pores was parallel to the loading axis, while the other 2 sets were perpendicular to the loading axis. The tests were carried out on a servo-hydraulic load frame (MTS 4 post (44 KN)) under displacement control at a stroke rate of 1.27 mm/min keeping thick papers as compliant layers on the top and bottom plattens. One of the three pore geometry parameters W, H, and I was varied to vary the pore volume while the others were kept constant. The experimental volume fraction porosity ($\Phi_{expt.}$), measured with a mercury intrusion porosimeter (Autopore III, Micromeritrics, GA.) and Archimedes' method, varied over the range from 21 to 47%. The equivalent theoretical volume porosity (Φ_{th}) is calculated using Equation 1. Shrinkage along the radius and height of the cylindrical ceramic scaffolds was measured, and was found to be 8 and 11%, respectively. The processing and composition of these ceramics is described elsewhere [24, 28]. Fig. 3b shows schematic of failure path in these ceramic structures during uniaxial compression testing. The porous ceramic strands split from the main structure as the ceramic failed elastically. In the stress-strain diagram, as expected, there was no sign for any plastic deformation. We also did not notice any mid-plane crushing with these structures.

6. Results

6.1. Macroscopic study of porosity

The experimental data plotted in Fig. 4 shows the cumulative variation of porosity due to different pore geometry. The results shown in Fig. 4 present a macroscopic viewpoint of strength degradation with increase in porosity. It is similar to that observed elsewhere for random porous ceramics [3, 32]. The mullite without fabricated macropores used in this study exhibited a measured density of 3.0 gm/cm^3. Compared to the theoretical density of 3.25 gm/cm^3, this indicates a microporosity of 8% due to incomplete sintering. This value is common for ceramic materials. These samples were tested in tension to evaluate the tensile strength of the dense ceramic.

The *ESIP* value is unity when there is no interaction between the stress fields of the pores for a particular material system. For the non-random porous system studied in this paper, the limiting *ESIP* value for no interaction can exist when no pores are present. For this particular condition the theoretical porosity is equal to zero ($\Phi_{th}, A_{th} = 0$). The *ESIP* value of unity thus obtained for $\Phi_{th}, A_{th} = 0$, multiplied by the same constant M, will give the tensile failure strength of a brittle solid.The value of M that correlates the theoretical and experimental results for a

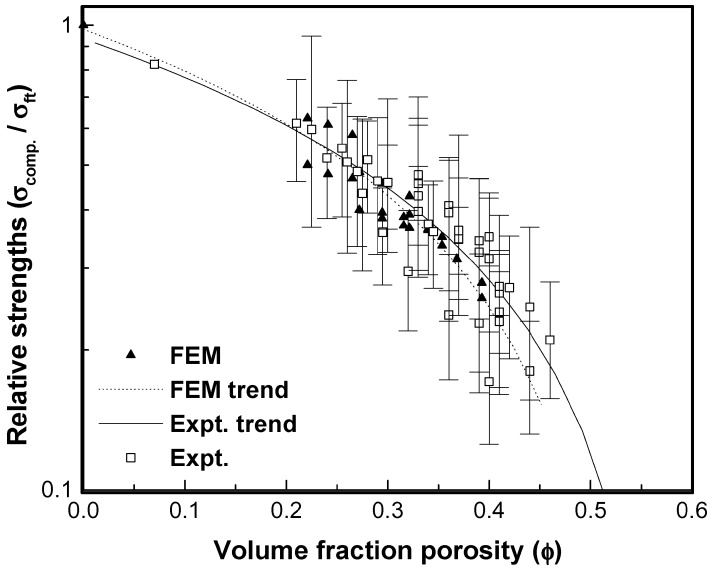

Figure 4 Cumulative failure strengths under compression as a function of volume fraction porosity.

different macroporosity obtained from different pore geometries is 91. From this discussion, the theoretical value of σ_{tension} at zero porosity is 91 MPa for the specific mullite system and processing condition that was adopted to fabricate the porous structure. However, the value of $\sigma_{\text{tension}} = 91$ MPa cannot be generalized for all mullite ceramics which are fabricated using other processing and surface finishing conditions. Nevertheless, for any particular processing condition a constant specific to that method can be obtained. Such a constant, when multiplied by the *ESIP* value, will give the compressive failure stress of a 3D honeycomb porous ceramic that has been processed by that particular method.

The compressive strength depends on structural parameters, e.g., grain shape, orientation and size [3]. When porosity is induced by partial sintering methods, these parameters play a significant role in the determination of compressive strength as Φ approaches *zero*. In this paper, the sintering cycle was maintained constant and all samples were processed by slurry casting in polymer molds generated via FDM (lost-mold technique). The microporosity induced by incomplete sintering was maintained constant for all 3D honeycomb structures.

6.2. Weibull parameters

The test results shown in Fig. 4 display some scatter, probably caused by imperfections in the porous ceramic. The failure stress can be characterized by an equation with the form associated with a Weibull distribution [33].

$$\ln\left(\ln\left(\frac{1}{S}\right)\right) = m \ln\left(\frac{\sigma}{\sigma_0}\right) \tag{10}$$

In Equation 10 S is the survival probability, the fraction of samples that would survive a given failure stress σ, and m is the Weibull modulus. The normalizing stress σ_0 is the stress at which the survival probability is $1/e = 0.37$ for a specimen of volume N. The survival probability for jth specimen is given by Equation 11,

$$S_{\text{j}} = 1 - \frac{j - 0.3}{N + 0.4} \tag{11}$$

In this paper, the number of samples, N, for any particular porosity were 10–12 specimens. Fig. 5 shows the plot of Weibull modulus m for compressive failure stress as a function of porosity. The mean Weibull modulus m was **5.7** with a standard deviation of **1.5**. These values of Weibull modulus are comparable to those observed for tensile and compressive strength of partially sintered porous ceramics ($m_{\text{ten.}} \sim 7$, $m_{\text{comp.}} \sim$ 3–6) and tensile strength of aluminum foams ($m \sim 7$) [3, 11]. In the following sections the porosity variations for different pore geometry parameters are analyzed in detail.

6.3. Microscopic study of pore parameters

The processing method adopted allows the variation of volume fraction porosity (Φ) by varying either W or H or I or by a combination of the parameters shown in Fig. 1. Hence porosity can be said to be an explicit function of W, H and I and expressed as an explicit relation,

$$\Phi = f(W, H, I) \tag{12}$$

The porosity (Φ) can also be varied by varying pore shape and size. The pore shape (S) can be varied by changing W or H and is thus an explicit function of W, H. The pore size variation (Z) can be of uniform or non-uniform nature. The uniform variation can be achieved by explicitly varying W and H simultaneously. The non-uniform variation of pore size is same as pore shape (S) variation. Hence pore size (Z) is an explicit function of W/H and S. Therefore Φ is an implicit function of S, Z and I and expressed as an implicit relation,

$$\Phi = f(S, Z, I) \tag{13}$$

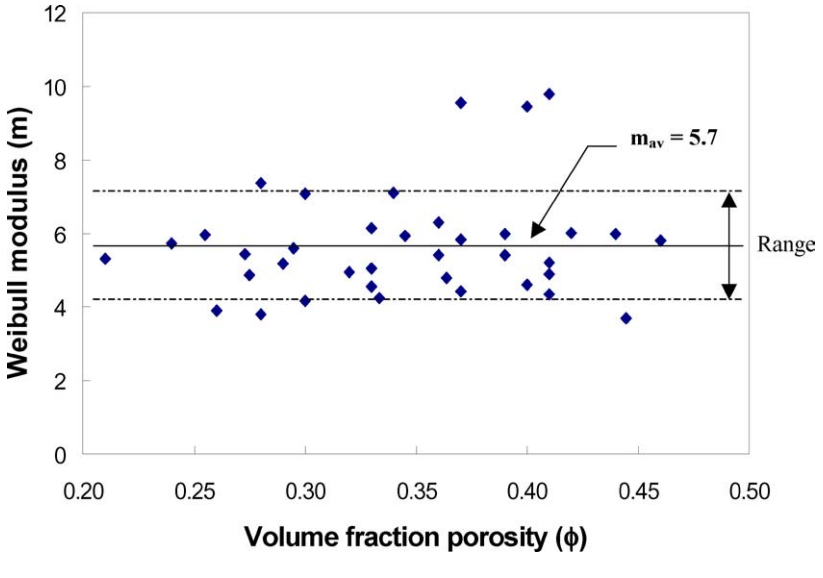

Figure 5 Weibull modulus m for failure compressive stress values for different porosities.

where

$$Z = f(W/H, S), \quad S = f(W, H)$$

6.3.1. Porosity variation due to pore-pore horizontal interaction distance

In this case, variation in porosity (Φ) is obtained by only varying pore interaction distance (I). This is an explicit analysis variation of porosity, where pore width (W) and pore height (H) are maintained constant and the porosity is expressed as $\Phi = f(I)$. By changing I, horizontal ceramic width between adjacent pores in Figs 6 and 7 is changed. As I is increased, the volume fraction porosity (Φ) is decreased and the stress interaction activity between pores is found to be reduced; this increases the failure strength of the ceramic structure. Figs 6 and 7 show the dependence between failure stress and porosity (Φ).

In Fig. 6, the two curves represent variation of porosity (Φ) for two different W values. It may also be noticed that the $W : H$ ratio is different for the two curves. The data in *Curve 2* are for a pore shape which is almost circular, and show a higher strength than exhibited by *Curve 1*. But it may be worth noting here that although the pore ellipticity is decreased as W is decreased, Φ is reduced too. Hence the effect of pore shape is not easy to separate in these curves.

Fig. 7 shows the two curves, which represent change in porosity (Φ) for two different H values. In this case according to Equation 9, Φ_{th} is independent of H, but the experimental results indicate that H has some effect on Φ. The strength of the structures decreases as Φ increases. Similar to the previous case, it can also be noticed that the $W : H$ ratio is different for the two curves and though the pore ellipticity decreases, Φ is also reduced. Therefore the effect due to change in pore width (W) on porosity (Φ) is not clear.

6.3.2. Porosity variation due to pore width

In the data shown in Figs 8 and 9, Φ is varied by variation of pore width (W) alone. Figs 8 and 9 show the dependence between failure stress and porosity (Φ).

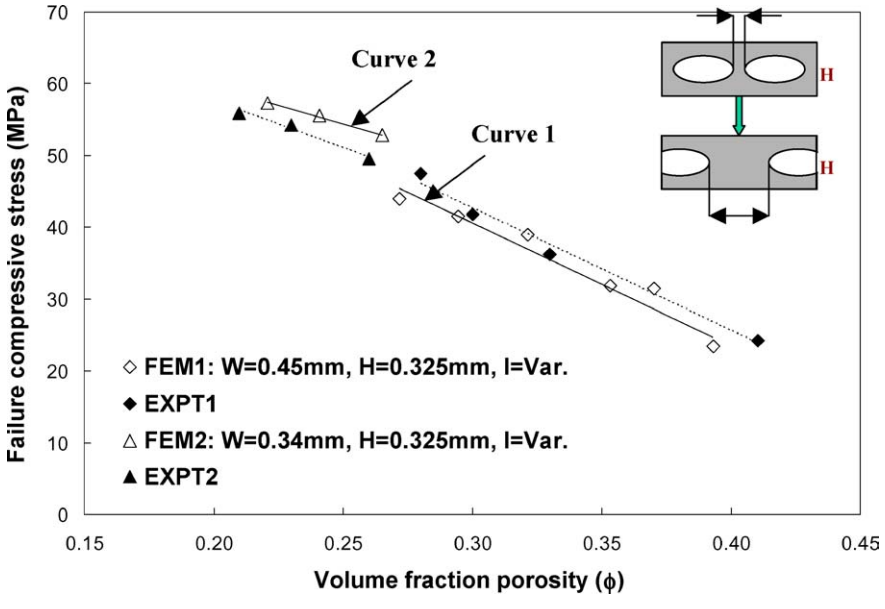

Figure 6 Variation of $\Phi = f(I)$, where W, H = Constant. Two values shown for two values of W.

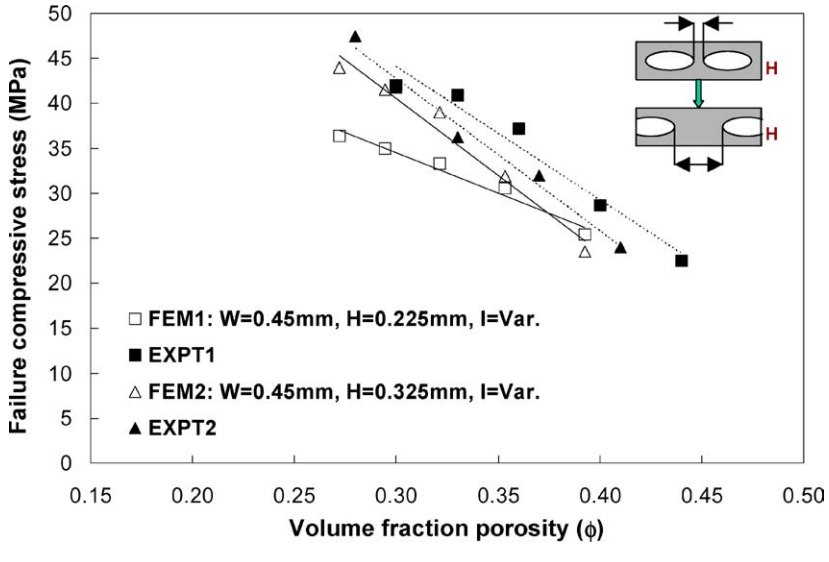

Figure 7 Variation of $\Phi = f(I)$, where W, H = Constant. Two values shown for two values of H.

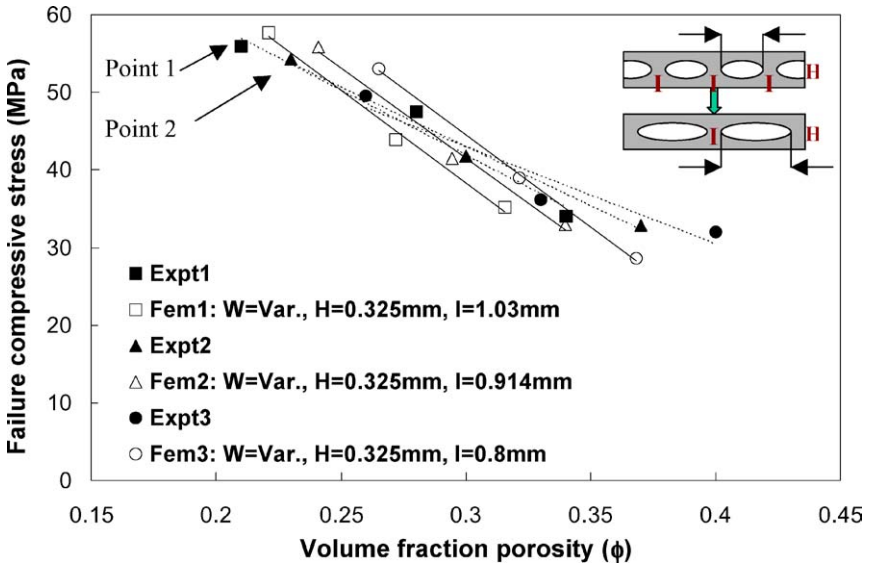

Figure 8 Variation of $\Phi = f(W)$, where H, I = Constant. Curves are shown for three values of I.

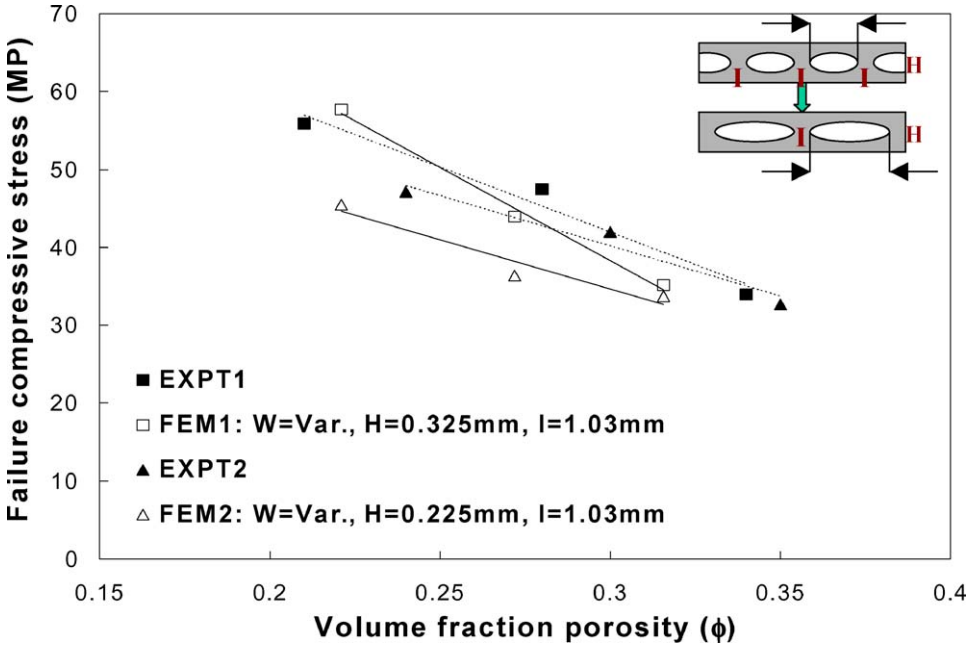

Figure 9 Variation of $\Phi = f(W)$, where H, I = Constant. Two curves shown for two values of H.

The two curves shown in Fig. 8 for variations of porosity (Φ) are for two different I values. In this variation of porosity, where pore height (H) and pore-pore interaction (I) are kept constant, the porosity is expressed only as a function of W. By increasing W and keeping H constant, the pore in Fig. 1 is made more elliptical in the horizontal direction, which increases Φ. Changing pore width also causes a change in pore shape (S) and a non-uniform change in pore size (Z). In other words, this involves a variation of porosity, which is a function of S, Z. As the horizontal ellipticity increases, stress interaction between pores is found to decrease slightly. Although this reduces the strength, the reduction is mainly due to the change in pore shape and pore volume. The exact contributions are not clear from these experimental results, which can be observed from point 1 and 2.

Fig. 9 shows two curves for variation of porosity (Φ) for two different H values. As observed earlier, H affects Φ as shown by the experimental results. It is seen that as Φ increases, the difference in strength is reduced for the two curves. This effect is also observed, to a lesser degree, in the experimental results.

6.3.3. Porosity variation due to pore height

Variation in porosity (Φ) can be obtained by varying pore height (H). In this porosity variation, pore width (W) and pore-pore interaction (I) are kept constant and the porosity is expressed as $\Phi = f(H)$. By increasing H and keeping W constant, the pore in Fig. 1 is made more elliptical in the vertical direction, proportionately increasing Φ. Pore height variation also causes a change in pore shape (S) and non-uniform change in pore size

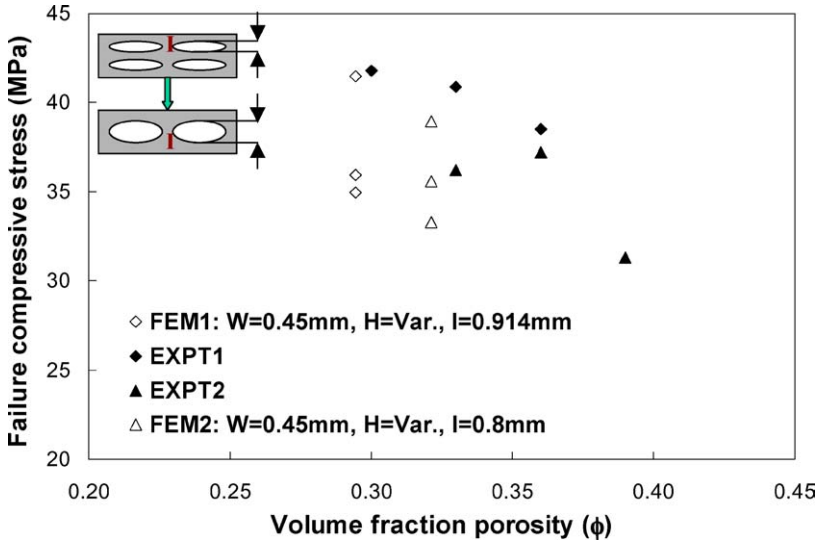

Figure 10 Variation of $\Phi = f(H)$, where W, I = Constant. Values shown for two values of I.

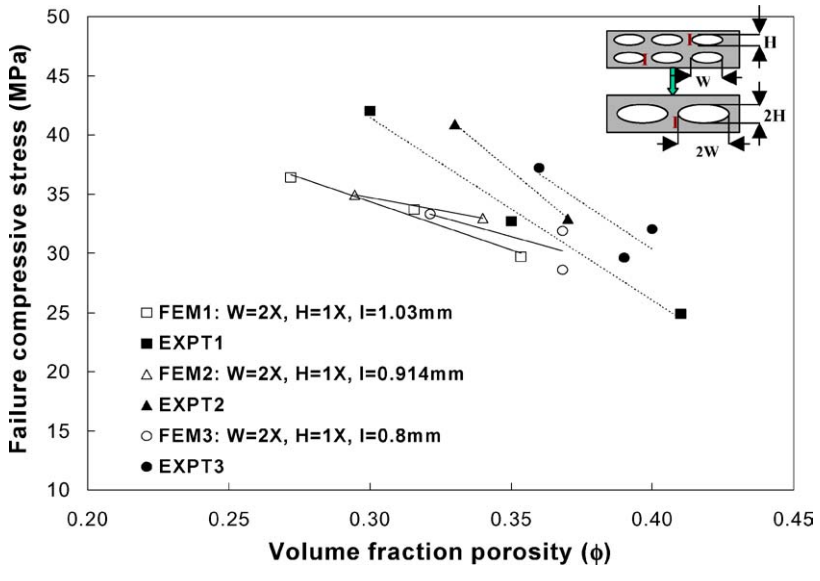

Figure 11 Variation of $\Phi = f(Z)$ where S, I = Constant. Curves are shown for three values of I.

(Z). This case involves an implicit variation of porosity; according to Equation 13 Φ is also a function of S, Z. As observed earlier, the effects of pore heights (H) on porosity (Φ) are shown by the experimental results in Fig. 10. Fig. 10 shows the dependence between failure stress and porosity (Φ). The two curves in Fig. 10 for variation of Φ are for two different values of I. The FEM values do not indicate a change with porosity.

6.3.4. Porosity variation due to pore size

Varying pore width (W) and pore height (H) simultaneously also varies the pore size (Z) and the porosity (Φ). This is an implicit variation of porosity, in which pore shape (S) and pore interaction (I) are maintained constant and porosity is expressed by Equation 13 as $\Phi = f(Z)$. The shape ratio $W:H$ is kept a constant at 2:1. Fig. 11 shows the dependence between failure stress and porosity (Φ). The three curves in Fig. 11 for the variation in Φ are for three different values of I. The trends remain the same for different values of I as shown by the 3 sets of curves in Fig. 11.

7. Discussion

The modeling approach presented in this paper predicts the failure stresses of three-dimensional honeycomb porous ceramics. Using the two-pore model illustrated in Fig. 3 quantitative values of failure stresses under compression are obtained. The theoretical porosity is obtained using Equation 9 and the theoretical values of failure stress are obtained using the procedure outlined. There is *no* empirical relation or curve fitting parameter that is adopted to relate the theoretical and experimental results. The analysis uses principles of mechanics to evaluate stress interactions due to neighboring pores. It also predicts the stresses for porosity variations due to the pore-geometry parameters shown in Figs 6–11 for porosities from 21–45 vol%.

The analysis in this paper shows that there is a change in strength due to a change in volume fraction porosity. The change in porosity can be caused by the different pore parameters. One of the modeling approaches of porous ceramics considers only the minimum solid area (*MSA*) [34, 35]. It can be observed from the discussion

presented here that in non-random porous ceramics the pore interaction distance (I) represents the *MSA*. Figs 6 and 7 show the variation of strength due to I. It should be emphasized that the change in pore width (W) is also an important parameter, since it causes change in shape (S) and the non-uniform change in size (Z) shown in Figs 8 and 9. The effect of W should be accounted for while modeling a porous material, although it is difficult to predict the exact contribution of W and I on strength degradation.

It is observed from Equation 9 that the theoretical volume fraction porosity (Φ_{th}) as a function of pore geometry parameters is independent of pore height (H). The experimental results of pore parameter variations in Figs 7, 9 and 10 show that the actual porosity (Φ_{expt}) is affected by pore height (H). This may be due to various reasons, including tolerances of the FD process while making molds and differential shrinkage after the sintering process of the ceramic structures. The analytical fracture mechanics approach qualitatively highlights the importance of pore parameter for different volume porosity. Though the FEM does not compare quantitatively with the analytical results it does bring out the importance of pore parameter on failure strength of porous ceramics. Therefore a qualitative similarity can be deduced between the two modeling approaches.

7.1. Limitations using the FEM approach

When the ellipticity of the pores become large, $W : H >$ 2.5, the ratios of stress concentrations between compressive and tensile stresses predicted by FEM tends to become larger than 10 : 1. In such a case, the nature of failure in the samples may be different than shown in Fig. 3. This is because the porous ceramic loaded in uniaxial compression may fail due to compressive stresses rather than tensile stresses, contrary to the discussion provided in this paper. The modeling approach adopted in this paper may not be appropriate for certain honeycomb brittle ceramics in which stress ratio (R) is less or pore ellipticity is higher, $R_{pore} > 10 : 1$. Similar inaccuracies in stress predictions may be noticed when in the vertical direction the distance between pores decrease and the pores are very close. The FEM results may not clearly predict the stress values, since the *ESIP* values are large because of the close stress interactions.

7.2. Microstructural material issues

All three-dimensional honeycomb structures not only had porosity which was designed (macroporosity), but porosity as well, which was due to incomplete sintering (microporosity). In this study these amounted to ~8%, as indicated. The modeling considered only idealized shapes without microporosity. A quantitative correlation suggests that if the microporosity in a porous material is kept to a minimum, the approach can be used effectively. It also suggests that microporosity does not play as significant a role as do designed macropores in the failure of porous materials if the density is near theoretical values.

The *ESIP* value for no interaction between pores is unity, which is observed when the stress fields between pores do not interact. It does not necessarily mean that the porosity should be zero to observe no interaction between the stress fields. Although in non-random porous structures this case can occur when the theoretical porosity is zero, such need not be the only case. It is possible that the *ESIP* value is unity when the porosity is between zero and residual value (~8%). The theoretical tensile failure stress obtained as 91 MPa in this paper therefore cannot be generalized to all mullite systems. The actual theoretical value of tensile strength at zero porosity is difficult to obtain. The approach presented here provides a convenient solution to evaluate the theoretical tensile strength of the solid at near zero porosity. It is not clear how the procedure can be extrapolated to model random porous brittle solids. Moreover, the behavior of non-random porous brittle solids has only been analyzed from stress interaction effects. The method of handling cracks and their growth from cylindrical pore under compressive stress has been proposed elsewhere [18, 29]. The results and theoretical methodology adopted in this paper are consistent with the theory of crack interactions [37]. The experimental results in this study show that stresses interact with surfaces of a finite sample in a way which causes them to grow faster than they do in an infinite medium.

This paper presents a methodology, which can be used to predict the compressive failure strength of porous ceramics, regardless of different pore geometries. An argument quoted earlier, that of the interactive nature of stress concentrations with increasing porosity, has been considered.

8. Conclusions

Three-dimensional honeycomb porous structures have been processed through a fused deposition process. A numerical approach using the FEM is presented to model these structures for pore geometry by evaluating elastic stress interactions between pores. It was observed that the stress interaction values can be multiplied by the tensile failure stress ($\sigma_{tension}$) to give failure stress under compression. Experimental and theoretical correlations for pore geometry are shown for porosity from 0 to 50 volume percent. The use of empirical relations or curve fitting parameters is not necessary.

It was found that microporosity does not play as significant a role in the failure of porous materials as do the designed macropores when density is near to theoretical. Since behavior of brittle porous solids in compression is complicated, the paper does not arrive at a complete description, although the behavior of non-random porous solids was analyzed in detail. This paper provides an analysis of the interaction of stress concentration with increasing porosity, and its effect on strength when pores are no longer isolated.

An analytical fracture model is presented which corroborates the need to address importance of pore parameters for different pore densities. It identifies the critical role played in failure mechanisms by pore shape

in high density solids and pore-pore spacing in low density solids. The FEM approach extends the analytical concept and presents a convenient method to model failure of designed porosity in ceramics. The FE modeling identifies that pore shape along with pore-pore interaction distance can cause failure especially when porosity is largely dependent on both. Experimental verification of the model asserts this viewpoint.

Acknowledgements

Financial support from the Office of Naval Research (ONR) under grant number N-00014-98-1-0550 [Program Manager: Dr. Steve Fishman] is acknowledged. The authors would like to acknowledge the experimental and processing help of Mr. Raj Atisivan, Mr. Jens Darsell and Dr. Susmita Bose. For several stimulating discussions on this subject, authors would like to acknowledge Prof. Steve Antolovich of MME, WSU and Dr. Roy Rice.

References

1. R. M. DE SOUZA, H. N. YOSHIMURA, C. XAVIER and H. GOLDENSTEIN, *Key Engineering Materials* **127–131** (1997) 439.
2. L. J. GIBSON and M.F. ASHBY, "Cellular Solids: Structure and Properties," 2nd ed. (Cambridge University Press, Cambridge, U.K., 1997).
3. R. W. RICE, "Porosity of Ceramics" (Marcel Dekker Inc., New York, 1998).
4. R. RYSHKEWITCH, *J. Amer. Ceram. Soc.* **36**(2) (1953) 65.
5. W. DUCKWORTH, *ibid.* **36**(2) (1953) 68.
6. R. L. COBLE and W. D. KINGERY, *ibid.* **39**(11) (1956) 377.
7. D. C. C. LAM, F. F. LANGE and A. G. EVANS, *ibid.* **77**(8) (1994) 2113.
8. D. HARDY and D. J. GREEN, *J. Euro. Ceram. Soc.* **15** (1995) 769.
9. D. M. LIU, *Ceramics International* **23** (1997) 135.
10. A. RAVAGLIOLI and A. KRAJEWSKI, *Materials Science Forum* **250** (1997) 221.
11. K. Y. McCULLOUGH, N. A. FLECK and M. F. ASHBY, *Acta Mater.* **47**(8) (1999) 2323.
12. M. A. SADOWSKY and E. STERNBERG, *J. Appl. Mech.* (1949) 149.
13. A. R. BOCCACCINI, G. ONDRACEK, P. MAZILU and D. WINDELBERG, *J. Mech. Behav. Mater.* **4**(2) (1993) 119.
14. R. W. RICE, in "Treatise on Materials Science and Technology: Properties and Microstructure" (Academic Press, 1977) Vol. 11, p. 199.
15. A. G. EVANS, D. R. BISWAS and R. M. FULRATH, *Trans. J. Brit. Ceram. Soc.* **62**(1/2) (1979) 95.
16. R. W. ZIMMERMAN, "Compressibility of Sandstones" (Elsevier Science, Netherlands, 1991).
17. I. TSUKROV and M. KACHANOV, *Int. J. Solids Structures* **34**(22) (1997) 2887.
18. C. FOND, J. L. FLEJOU and Y. BERTHAUD, *Eur. J. Mech., A/Solids* **14**(1) (1995) 73.
19. L. J. GIBSON, M. F. ASHBY, G. S. SCHAJER and C. I. ROBERTSON, *Proc. R. Soc. London* A **382** (1982) 25.
20. L. J. GIBSON and M. F. ASHBY, *ibid.* **382** (1982) 43.
21. E. W. ANDREWS, L. J. GIBSON and M. F. ASHBY, *Acta Mater.* **47** (1999) 2853.
22. A. G. EVANS, J. W. HUTCHINSON and M. F. ASHBY, Harvard University Report, MECH-323, 1998.
23. A. HATTIANGADI and A. BANDYOPADHYAY, *Scripta Mater.* **42**(6) (2000) 581.
24. S. BOSE, S. SUGUIRA and A. BANDYOPADHYAY, *ibid.* **41**(9) (1999) 1009.
25. A. HATTIANGADI and A. BANDYOPADHYAY, *J. Amer. Ceram. Soc.* **83**(11) (2000) 2730.
26. A. BANDYOPADHYAY, R. K. PANDA, V. F. JANAS, M. K. AGARWALA, S. C. DANFORTH and A. SAFARI, *ibid.* **80** (1997) 1366.
27. R. ATISIVAN, A. HATTIANGADI, S. BOSE and A. BANDYOPADHYAY, *Ceramic Trans.* **103** (1999) 92.
28. R. ATISIVAN, S. BOSE and A. BANDYOPADHYAY, *J. Amer. Ceram. Soc.* **84**(1) (2001) 221.
29. C. G. SAMMIS and M. F. ASHBY, *Acta Metall.* **34**(3) (1986) 511.
30. M. F. ASHBY and S. D. HALLAM, *ibid.* **34**(3) (1986) 497.
31. ANSYS Ver. 5.4 User's Manual, 1996.
32. F. P. KNUDSEN, *J. Amer. Ceram. Soc.* **42**(8) (1959) 376.
33. W. WEIBULL, *J. Appl. Mech.* **18** (1951) 293.
34. R. W. RICE, *J. Mater. Sci.* **31** (1996) 102.
35. *Idem.*, *ibid.* **31** (1996) 1509.
36. A. HATTIANGADI, M. S. Thesis, Mechanical Eng., Washington State University, May 2000.
37. K. Y. LAM, B. COTTERELL and S. P. PHUA, *J. Amer. Ceram. Soc.* **74**(2) (1991) 352.

Received 28 February 2003
and accepted 6 April 2004